Journal of Colloid and Interface Science 562 (2020) 159–169

Contents lists available at ScienceDirect

Journal of Colloid and Interface Science

journal homepage: www.elsevier.com/locate/jcis

Relationship between wetting and capillary pressure in a crude oil/brine/rock system: From nano-scale to core-scale

M. Rücker [a,b,*], W.-B. Bartels [b,c], G. Garfi [d], M. Shams [d], T. Bultreys [a,e], M. Boone [f], S. Pieterse [b], G.C. Maitland [a], S. Krevor [d], V. Cnudde [e,c], H. Mahani [b], S. Berg [a,b,d], A. Georgiadis [a,b], P.F. Luckham [a]

[a] Chemical Engineering, Imperial College London, SW7 2AZ, UK
[b] Shell Global Solutions International B.V., 2288 GS Rijswijk, Netherlands
[c] Earth Sciences Department, Utrecht University, 3584 CD Utrecht, Netherlands
[d] Earth Science and Engineering, Imperial College London, SW7 2AZ, UK
[e] UGCT-PProGRess, Ghent University, Krijgslaan 281 S8, 9000 Ghent, Belgium
[f] TESCAN XRE, Bollenbergen 2B Bus 1, 9052 Gent, Belgium

GRAPHICAL ABSTRACT

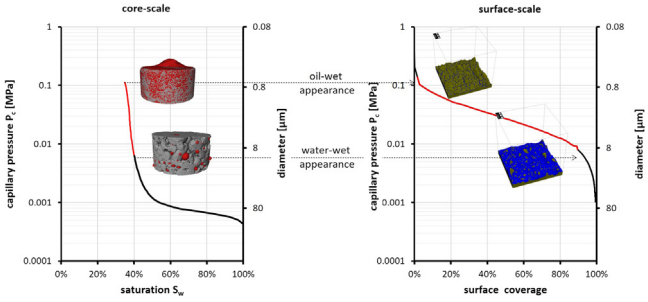

ARTICLE INFO

Article history:
Received 10 September 2019
Revised 19 November 2019
Accepted 19 November 2019
Available online 21 November 2019

Keywords:
Surface roughness
Wetting
Atomic force microscopy (AFM)
Core initialization
Capillary pressure
Disjoining pressure

ABSTRACT

Hypothesis: The wetting behaviour is a key property of a porous medium that controls hydraulic conductivity in multiphase flow. While many porous materials, such as hydrocarbon reservoir rocks, are initially wetted by the aqueous phase, surface active components within the non-wetting phase can alter the wetting state of the solid. Close to the saturation endpoints wetting phase fluid films of nanometre thickness impact the wetting alteration process. The properties of these films depend on the chemical characteristics of the system. Here we demonstrate that surface texture can be equally important and introduce a novel workflow to characterize the wetting state of a porous medium.

Experiments: We investigated the formation of fluid films along a rock surface imaged with atomic force microscopy using ζ-potential measurements and a computational model for drainage. The results were compared to spontaneous imbibition test to link sub-pore-scale and core-scale wetting characteristics of the rock.

Findings: The results show a dependency between surface coverage by oil, which controls the wetting alteration, and the macroscopic wetting response. The surface-area coverage is dependent on the capillary pressure applied during primary drainage. Close to the saturation endpoint, where the change in saturation was minor, the oil-solid contact changed more than 80%.

Abbreviations: AFM, atomic force microscopy; COBR, crude oil, brine, rock; DLVO, Derjaguin-Landau-Verwey-Overbeek; TAN, total acid number; TBN, total base number; SARA, Saturates, Aromatics, Resins, Asphaltene; USBM, U.S. Bureau of Mines; SCAL, Special Core Analysis; PV, pore volume.

* Corresponding author at: Chemical Engineering, Imperial College London, SW7 2AZ, UK.
E-mail address: m.rucker15@imperial.ac.uk (M. Rücker).

https://doi.org/10.1016/j.jcis.2019.11.086
0021-9797/

1. Introduction

Wetting describes the preference of a solid phase to be in contact with one fluid rather than another. In porous media, where the surface area of the solid phase is large, wetting is one of the controlling factors for two-phase flow, which plays a role in applications such as ink-jet printing, construction, soil infiltration, environmental remediation and oil recovery [1–9].

In an oil reservoir, which includes crude oil, brine and rock (COBR-system), a rock surface is called water-wet when the brine tends to cover it and is called oil-wet when it prefers to be in contact with the oil phase. The wetting of a rock may also vary from location to location. In this case the rock is called mixed-wet [10–15].

The flow behaviour in porous media is commonly characterised by capillary pressure-saturation- functions and relative permeability- saturation functions. So far these functions can only be determined through costly and time intense Darcy (core) -scale experiments (e.g. flooding). Pore-scale computational models and simulation approaches struggle for various reasons. Computational performance is one aspect, but more conceptually, it is currently not fully understood how to effectively characterize wetting behaviour of rock and assign a representative spatial distribution at the pore-network scale, on which basis a meaningful average could be computed to obtain a Darcy-level response. As a consequence, the exact relationship between wetting and the Darcy-scale response is not very well understood, in particular the impact of the spatial wetting distribution. The Darcy-scale wetting response is commonly characterized by indices derived from capillary pressure-saturation- functions, which are obtained by measuring the capillary pressure required to change the saturation within the porous medium [16–19]. The fluid phase which imbibes the sample spontaneously is thereby considered the more wetting phase [16,20]. However, wetting itself is a molecular scale property, determined by the molecular interactions of the three phases present. In order to upscale wetting, further parameters occurring at larger length scales need to be considered. One of these is the structural variation of the porous medium, which is dominant in chemically homogeneous carbonates forming 60% of the worldwide oil reservoirs. In addition to the general pore-geometry, surface roughness, which may for instance originate from the microporosity, may also influence the response [21–24,110,111]. However, so far, studies focussing on the impact of surface roughness on flow in permeable media, are either conceptual or demonstrate experimentally a relationship, but are missing the direct link allowing the upscaling of molecular characteristics to pore- and core-scale responses [24–31].

In this work, we assess the impact of the surface structure of natural rock on the core-scale wetting response by investigating the fluid distribution at different length scales and introduce a systematic workflow linking molecular phenomena with pore- and core-scale responses.

1.1. Wetting from the molecular scale to fluid films

Only a few minerals, such as graphite or talc are naturally hydrophobic [32,33]. Most minerals present in reservoir rock are originally strongly water-wet [34–36]. However, the wetting of a surface may be altered towards more oil-wet by precipitation and/or adsorption of surface-active components present in the crude [37–40]. Carbonate rock tends to become more oil-wet than sandstone, which is often attributed to the positive surface charge of calcite at reservoir conditions [15,34,41,42]. The interactions between different oil-components and the rock surface can be studied for instance with atomic force microscopy (AFM), in which the force required to pull off a probe of nano-scale size (radius r = 10–50 nm), the adhesion force, is measured [35,43].

In addition to the chemistry of the crude oil and the surface chemistry of the rock, the brine composition also impacts wetting [44,45]. On a mineral surface covered with brine, the balance between electrostatic forces and van der Waals forces leads to a double layer of counterions in correspondence with Derjaguin-Landau-Verwey-Overbeek (DLVO theory; [46,47]), which impacts the repulsive/attractive forces of approaching oil-molecules [48,49]. In combination with structural forces of the fluid/fluid interface these lead to a disjoining pressure Π given by:

$$\Pi(\mathbf{h}) = -\frac{\delta(\boldsymbol{W_{VDW}} + \boldsymbol{W_{el}} + \boldsymbol{W_{st}})}{\delta \boldsymbol{h}} \tag{1}$$

with the work related to van der Waals forces W_{VDW}, electrostatic forces W_{el} and structural forces W_{st}, and thickness of the water film δh [48,50].

The Van der Waals force is usually attractive and correspondingly, contributes to a negative capillary pressure and destabilization of the water film. The structural force is always repulsive, contributing to positive disjoining pressure which stabilizes a water film. However, electrostatic forces, which can be assessed with ζ-potential measurements, can have a negative or positive contribution to disjoining pressure [27,51]. If the surface charges of the rock surface and the fluid-fluid interface are attractive, the water film is unstable and the overall disjoining pressure remains negative as illustrated by the dotted disjoining pressure – film thickness function shown in Fig. 1B. For repulsive surface charges, the positive contribution of the electrostatic forces to the disjoining pressure, illustrated by the dashed line in Fig. 1B, causes a stabilization of the water film. The film ruptures if the maximum disjoining pressure Π^{max} is exceeded [27]. Only if the water film ruptures, the non-wetting phase can come in contact with the solid and allow the wetting of the surface to be altered [31]. In a mixed-wet system, the disjoining pressure must have been exceeded in some locations, but not in all [14,40]. Chemical heterogeneity may be one reason for variation in disjoining pressure [31]. However, carbonate rocks are dominated by calcite or dolomite, which makes them mostly chemically homogeneous. Mineral variation is therefore unlikely to be generally responsible for the wetting variation in this rock. Correspondingly, the structure of the rock, given by the pore geometry and surface roughness, is controlling the mixed-wet behaviour, which is commonly assessed at the core-scale.

1.2. Wetting from the core- to the pore scale

Within the confined space of porous media wetting is reflected by the term capillary pressure, P_c given by the Young-Laplace equation:

$$\boldsymbol{P_c} = \boldsymbol{P_o} - \boldsymbol{P_b} = \sigma^{\boldsymbol{ob}}\kappa \tag{2}$$

with $\boldsymbol{P_o}$ and $\boldsymbol{P_b}$ being the pressure of the oil and brine phases respectively, $\sigma^{\boldsymbol{ob}}$ the interfacial tension between oil and brine and the total curvature κ of the oil-brine interface. For static conditions this equation can be rephrased to:

$$\boldsymbol{P_c} = \frac{2\sigma^{\boldsymbol{ob}}\mathbf{cos}(\theta)}{\boldsymbol{r}} \tag{3}$$

with θ being the contact angle between the oil, brine and rock surfaces measured perpendicular to the three-phase contact line through the denser phase and r the radius of the pore.

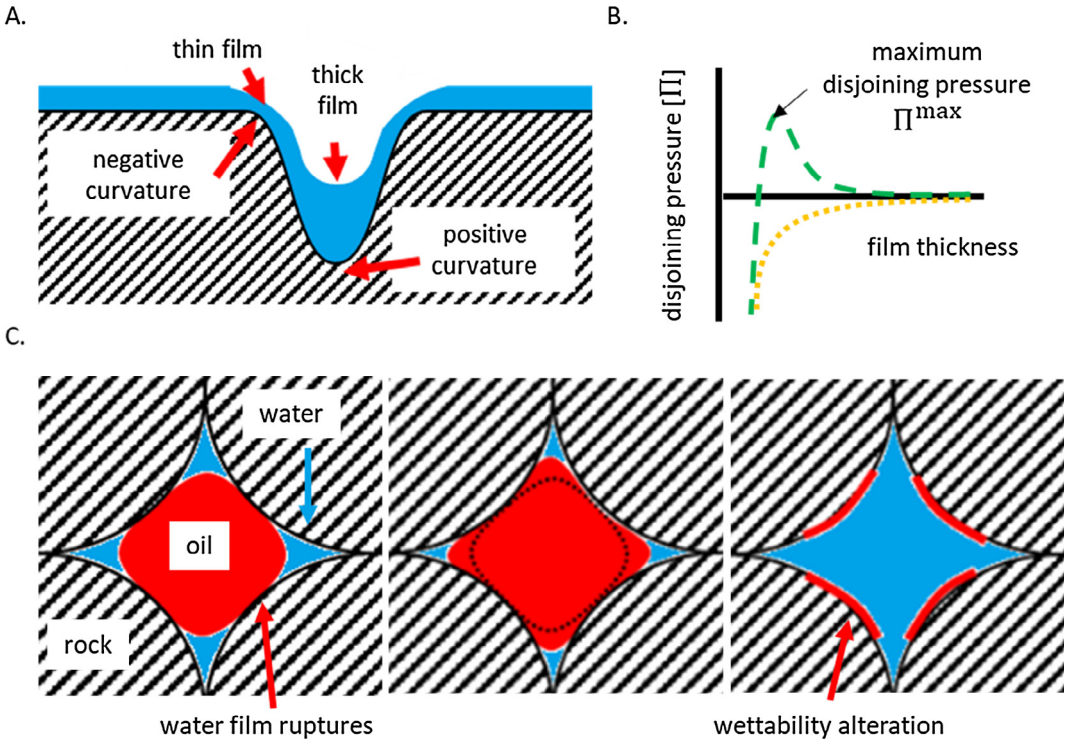

Fig. 1. (A) illustrates the distribution of a water film for a constant global capillary pressure P_c^* along a surface with varying structure. The difference in curvature leads to a different local capillary pressure P_c^{local} and correspondingly to variation in film thickness. Based on the augmented Young-Laplace equation (IV) negative surface curvature leads to a thinner film, while positive surface curvature causes a thicker film. The stability of the film is given through the disjoining pressure – film thickness relationship (B). Depending on the fluid-fluid-rock system, this relationship may reflect repulsive (green) or attractive (yellow) interactions between the fluid-fluid and the fluid-solid interface. Only if the interfaces are repulsive disjoining pressure stabilizes the fluid film up to the point the maximum disjoining pressure is exceeded by the local capillary pressure, where the film ruptures (C-left). Once the water film ruptured, the invasion depth controls which surfaces are covered with oil and with water (C-centre). After ageing these surfaces remain oil-wet, even when the oil present is replaced by brine (C-right). (For interpretation of the references to colour in this figure legend, the reader is referred to the web version of this article.)

In conventional Darcy-scale experiments, the capillary pressure is reported as a function of saturation. Down to a capillary pressure of zero the capillary pressure -saturation relationship is derived from the Amott spontaneous imbibition test in which the cumulative production versus time is recorded. The forced part at $\boldsymbol{P_c} < 0$ can be obtained from waterfloods. Various indices have been introduced to characterize wetting based on the capillary pressure saturation relationship from which the Amott and USBM (U.S. Bureau of Mines) indices are the most common [16,19]. However, the results of such experiments are difficult to interpret as other factors besides wetting may impact the results. These factors include e.g. viscosity, interfacial tension and flow dynamics. Various scaling groups have been introduced to achieve a better comparison [18,52,112]. Yet, these have only been proven effective for systems with a homogeneous wetting [52].

In recent years micro-computed tomographic imaging (μCT) techniques have been developed to complement core-scale experiments [53–67]. The in-situ visualization of the fluid phases allows the characterisation of the fluid distribution within the rock through the integral geometry and a set of morphological descriptors, the 4 Minkowski functionals [68]. The 4 Minkowski functionals include volume, surface area, curvature and topology (Euler characteristic) of the fluid phases. Based on Hadwiger's completeness theorem the 4 Minkowski functionals of any global morphology show a unique combination and form the only motion-invariant, conditional continuous and additive functional of this structure [69]. Describing a structure using Minkowski functionals simplifies the study of the relationship between structure and various properties, such as the energy of interfaces [70,71] or permeability of a porous medium [72,73], and also describes changes in structure, such as the change in fluid distribution during multiphase flow in rocks. Various studies targeted the relationship of fluid distributions occurring during two-phase flow to the pore-scale rock structure, to each other and to wetting [74–81] using the 4 Minkowski functionals and some studied the relationship between these parameters and core-scale properties like relative permeability - and capillary pressure – saturation relationships [56,66,76,82–86]. While these parameters were found to be key to upscale the flow-behaviour observed at the pore-scale to the core-scale, the link between the molecular wetting property and the fluid distributions occurring during two-phase flow and the corresponding Minkowski functionals remains unknown.

Another way to characterize the wetting of a rock is through in-situ contact angle measurements [57,86–89]. However, the contact angle values obtained do not deliver one single index for wetting, but a distribution of contact angles with one or multiple peaks. Even in homogeneous-wet systems, surface roughness can cause contact angle hysteresis, which leads to a range of different contact angles [90]. In a model system with controlled roughness and flow this effect can be described through an advancing and a receding contact angle [91,92]. In-situ in rock, in which surface structure may vary from location to location and in which the flow dynamics during and prior to the data acquisition at the pore level are unknown, the contact angle measured may show any value in between the advancing and a receding contact angle [25,93].

While the problems associated with core and pore-scale wetting characterization mostly result from the flow dynamics (advancing and receding menisci or fluid entrapment) affecting the measurement, the establishment of the wetting behaviour in the rock is commonly induced under static conditions. The

water-wet rock sample is drained to a specific capillary pressure and then aged for 3–6 weeks at elevated pressure and temperature [94]. The oil is thereby, expected to alter the rock surface where the two phases are in contact, as illustrated in Fig. 1 [26,31,40]. Correspondingly, the fluid distribution during ageing may induce a mixed- wetting even in chemically homogenous rocks such as the aforementioned carbonates.

The location at which the oil comes in contact with the rock can be derived from the augmented Young-Laplace equation given by:

$$P_c^* = \underset{P_c^{local}}{\sigma^{ob}\kappa} + \Pi(h), \tag{4}$$

for which, we observe an oil brine interface with a distance h from the solid surface following a grain surface with a varying curvature κ. To maintain a fixed global capillary pressure $\boldsymbol{P_c^*}$ the disjoining pressure must increase as the curvature of the interface (and grain) becomes negative and decrease when it is positive.

Depending on the disjoining pressure - film thickness relationship, the fluid may be maintained up to the point Π^{max} is reached (Fig. 1B, dashed line). Correspondingly, the films along protrusions become thinner and thicker in indentations as a variation of different local capillary pressures $\boldsymbol{P_c^{local}}$ is observed [31].

As the film ruptures at the point at which Π^{max} is reached, the film would break, where the curvature of the rock surface approached by the oil interface is highest and consecutively alter the wetting where in contact (Fig. 1). Commonly, only the grain sizes and the corresponding pore shapes are considered when the wetting pattern is simulated [30]. However, features along the grain that determine the surface roughness are likely to cause a much larger curvature variation than the grain shapes by themselves. Also, as Kovscek et al. [31] highlighted, the surface structure of rock would be of relevance for the wetting pattern observed if the protrusion length scale of asperities is much larger than the film thickness.

In the presented study we investigated the molecular interactions of the COBR system and the surface structure of a rock, analysed its impact on the nano-scale integral geometry of the oil phase and linked the results to core-scale behaviour. More specifically, we investigate the wetting behaviour we have observed in μCT experiments on core-scale samples based on the rock structure/pore geometry and compare that to what wetting behaviour is expected when including the surface structure on the grains measured by AFM. Our main goal is to describe to what extent the overall wettability state is determined by fluid occupancy of the nanoscale roughness or by fluid occupancy of the micrometer scale pore geometry.

2. Materials and methods

2.1. Fluids and rock samples

Ketton rock, quarried from the Ketton quarry in Rutland, England, is a middle Jurassic oolithic carbonate rock consisting of round grains (Ooids and peloids) ranging from 100 μm to 1 mm size which again contain an additional micro-porosity. Oolites are marine sediments, which form during evaporation of the sea. The dissolved carbonate in the seawater starts to precipitate along nuclei. Concentric growth and continues movement of the particles before deposition leads to the round shape of the grains [95]. Correspondingly the investigated surfaces within the rock may contain both, facets resulting from the initial growth and facets resulting from mechanical or chemical modifications afterwards. The rock history implies a homogeneous structure of the rock within the coring range of the samples obtained for this study (40 cm × 40 cm × 40 cm).

The pore size distribution of Ketton rock was assessed with Hg-porosimetry. The rock has a porosity of φ = 23% and permeability of 3–6 D. It consists predominantly of calcite (99,1%) with minor quartz (0.9%) components [96]. We assume a relative permittivity of 7, typical for carbonates [51]. While the rock is chemically homogeneous, the structure of rock can be considered complex, though typical for carbonates, because of the dual-porosity [95].

The crude oil was chosen based on its high wetting alteration potential, which was assessed by the total acid number (TAN) and the total base number (TBN) as well as by a SARA analysis. The results are shown in Tables 1 and 2. The crude oil is rich in surface-active components as well as asphaltenes, which represent the components which are expected to change the wetting of the rock since they have the capacity to absorb on to the rock surface.

For the μCT measurements, the crude oil was doped with 20% -iododecane, which caused the crude oil to appear in μCT within the same range of grey values as rock. This mixture results in the highest contrast between the two fluids (brine and oil), while the attenuation remains on the level of the rock.

The brine composition used in this study is listed in Table 3. The formation water recipe is typical to a carbonate reservoir [97].

The interfacial tension between the doped oil and brine was σ^{ob} = 20 mN/m at 25 °C.

2.2. Atomic force microscopy (AFM)

The surface structure of Ketton rock was assessed with AFM. In contrast to traditional microscopes, which create a magnified image by focusing electromagnetic radiation, such as photons or electrons. AFM images mechanically. An atomically sharp tip attached to the end of a cantilever is raster-scanned over a surface. The tip interacts with the underlying surface through various intermolecular forces. These forces lead to a bending of the cantilever, which is monitored by a laser, as illustrated in Fig. 2. This technique allows a very precise 3D visualization of the topography of a surface and also the detection of various physical properties.

In this study we used AFM (Nanowizard 4, JPK Instruments, now Brucker) to image the structure of the rock surface down to nanometer resolution. The measurements were conducted in approachable pores at the outer space of the Ketton sample not affected by drilling. The sample was scanned with a silicon tip (PPP-NCHAuD from NANOSENSORS™) on 50 μm × 50 μm area with a resolution of 512 × 512 pixel in Quantitative Imaging™ -mode. The image was levelled, filtered using a median filter, analysed for curvature and roughness and visualized with JPKSPM data processing software (JPK instruments) and then transformed into a 3D image with a voxel size of 0.097 μm using MATLAB (R2018b). This image was then further processed with AVIZO (ThermoFisher) for visualization of the curvature and GeoDICT 2015 (Math2Market, Kaiserslautern, Germany) to perform a drainage simulation and for visualization of the fluid films.

2.3. ζ-potential measurements

The presented ζ-potential measurements were carried out with a Zetasizer Nano-ZS (Malvern Instruments), which detects the electrophoretic mobility of particles within a suspension or oil droplets dispersed in the studied brine. The ζ-potential is then derived from the electrophoretic mobility using the Smoluchowski approximation of Henry's equation [99]. The rock was first ground and then mixed with brine following the protocols described in Zhang and Austad [100] and the oil-brine emulsion was prepared following the protocols described in Mahani et al. [51]. The samples were allowed to equilibrate for one day before any measurements were taken. The measurements were performed at 25 °C at a pH of 5.7,

Table 1
Basic properties of the crude oil used in this study.

Oil	TAN [mg KOH g^{-1}]	TBN [mg kg^{-1}]	Relative permittivity	Viscosity 20 °C [mPa s]	Density 20 °C [g cm^{-3}]
Crude oil	0.4	2.9	2	17	0.85

Table 2
SARA fractions for the crude oil used in this work displayed in the relative weight of each compound class.

Oil	Saturates [wt%]	Aromatics [wt%]	Resins [wt%]	Asphaltenes [wt %]
Crude oil	52.08	39.06	7.96	0.91

Table 3
Composition of formation water (FW) used in this work.

Ion	Na^+	Mg^{2+}	Ca^{2+}	Cl^-	SO_4^{2-}	HCO_3^-	Relative permittivity	Ionic strength [mol/l]	pH
[mg/l]	49,898	3248	14,501	111,812	234	162	78.3	3.659	5.7

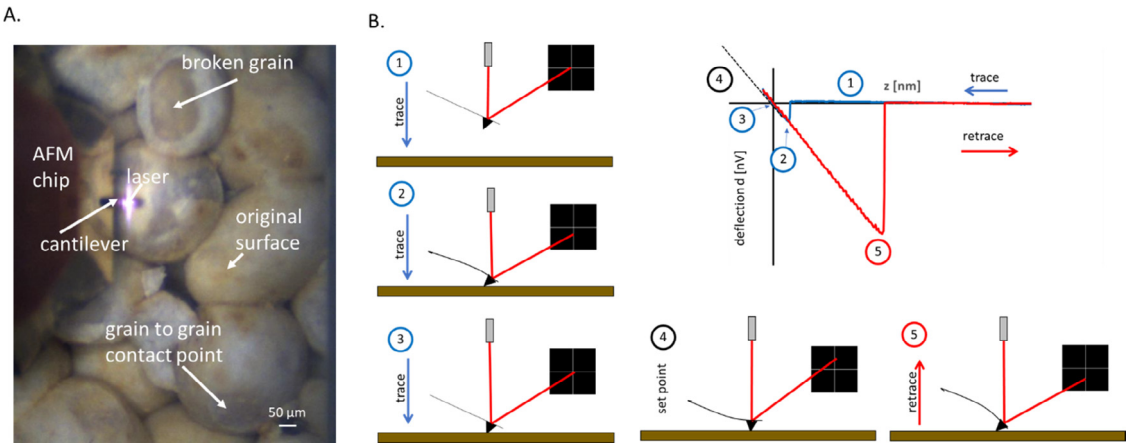

Fig. 2. Atomic force microscopy (AFM) was used to image the rock surface as it occurs within a pore (A). Atomic force microscopy operates with an atomically sharp tip, which is mounted on a cantilever and monitored by a laser. As the tip approaches and disengages the surface, the tip starts to interact with it causing a bending of the cantilever. The force-distance curves generated from the approach (trace) and disengaging processes (retrace) at each point scanned along the surface can then be used to visualize the surface topography and to determine other properties of the surface such as stiffness and adhesion (B) [98].

corresponding to the brine pH used in the core experiments. The results were used to calculate disjoining pressure – film thickness relationships following the procedure described in Mahani et al. [51].

2.4. Amott test

Amott spontaneous imbibition tests are simple experiments conducted at the core scale, which are often used for wetting determination [16,101]. In this test, an oil-saturated rock sample is placed into a vessel containing brine. In water-wet and mixed-wet samples the water spontaneously imbibes into the rock sample replacing the oil, which then gets produced. In an Amott vessel the produced oil is collected and monitored over time. The production rate and the overall production are used as a measure for wetting [102].

2.4.1. Sample initialization centrifuge

The Ketton rock sample (special core analysis (SCAL)-plug: diameter d = 2.5 cm and length L = 5 cm) was first saturated with brine (FW) and then desaturated with crude oil in a centrifuge (URC-628, 129 Coretest Systems Inc., used at 3500 RPM) for 24 h to reach initial water saturation S_{cw}. To counter the gradual heating during centrifugation, the temperature was kept constant at 40 °C with a heating element coupled with a temperature controller within the centrifuge chamber. During the experiment the production was continuously monitored. In addition, the sample was scanned using HECTOR a high energy µCT scanner at UGCT to visualize the fluid distribution within the sample. The voxel size achieved was 14.25 µm. A more detailed description of scanning settings and image processing can be found in Bartels et al. [88]

2.4.2. Sample initialization flow cell

The other Ketton rock sample (Mini-plug: diameter d = 4 mm and length L = 20 mm) was saturated with brine and desaturated by flooding oil with a flow rate of 1 mL/min (7.7 PV/min) for 193 PV (pore volume). The sample was scanned prior and after flooding with the Environmental µCT scanner (EMCT) at UGCT [103] with a voxel size of with 6.7 µm to assess the fluid distribution. Subsequently, the sample was placed into an oven at 40 °C for 24 h to mimic the same conditions as the SCAL plug. Due to the small volume of the sample, it was placed into the Amott cell without rolling it over a tissue. The production was again monitored using the Environmental µCT scanner with a voxel size of 13 µm. More details of the scanning settings and image processing can be found in Bartels et al. [88].

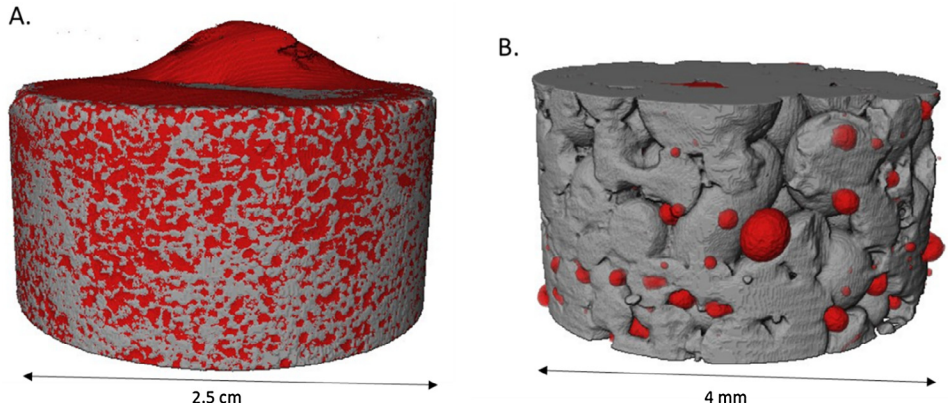

Fig. 3. μCT images showing the oil distribution (red) in Ketton limestone (rock). The oil droplets emerging from the rock during Amott spontaneous imbibition tests show a difference in shape, though the same COBR system was used. When initial by centrifugation the oil droplet spread over the rock surface indicating an oil-wet behaviour (A), while for samples initialized by flooding the droplet emerging indicated water-wet system (B).

3. Results and discussion

3.1. Wetting observations at the core scale

Macroscopic observation of the core samples revealed a difference in wetting, though the same COBR system was used. Fig. 3 shows the oil-phase droplets on the rock surface for the samples initialized by centrifugation (Fig. 3A) and flooding (Fig. 3B). The oil-droplet in Fig. 3A spreads over the sample surface, while the oil in Fig. 3B forms predominantly water-wet bubbles. This water-wet appearance has been reported for Ketton rock initialized by flooding in various previous studies [88,104]. Rücker et al. [105] observed with dynamic imaging that such water-wet appearing systems show flow behaviour typical for mixed-wet systems leaning towards the water-wet side. All these publications attribute this behaviour to the structure of Ketton rock.

The only difference between the samples appearing more oil-wet (Fig. 3A) and the samples appearing more water-wet (Fig. 3B) is the nature of the sample initialization, which is associated with a difference in capillary pressure. Based on the Young-Laplace equation (II), a difference in capillary pressure would result in a difference in fluid distribution as pores with a small diameter would not get filled at low capillary pressure but would at a high capillary pressure.

The capillary pressure achieved by centrifugation was 0.06 MPa at the bottom and 0.12 MPa at the top of the sample, which means that based on the Young-Laplace equation pores down to a size of 0.5–1 μm in diameter would be filled with oil as indicated in Fig. 4A showing the pore size distribution of Ketton rock. The zoomed-in μCT image, displayed in Fig. 4B of the SCAL sample (grey), shows a homogeneous distribution of the oil (also grey) with only little water remaining (black).

During initialization by flooding, the capillary pressure is controlled by the flow rate and the rock structure itself and therefore cannot be determined easily [94]. However, as illustrated in Fig. 4C, the oil is distributed homogeneously in the resolved large pore bodies and narrow pore throats, too. The few locations in which water remains trapped are likely related to flow dynamics. Correspondingly, the capillary pressure in the rock needs to be sufficient to fill all pores above, or close to, the resolution (voxel length: 6.7 μm).

Fig. 4A illustrates the range of pore-sizes which would be filled by centrifugation and the upper limit estimation for the sample initialized by flooding respectively. It becomes apparent that the two initialization methods would only cause minor differences in saturation. Therefore, the occupation of a pore by oil cannot be solely responsible for the wetting response observed at the core scale. Rücker et al. [105] hypothesized, that sub-resolution wetting patterns related to surface roughness may cause the water-wet

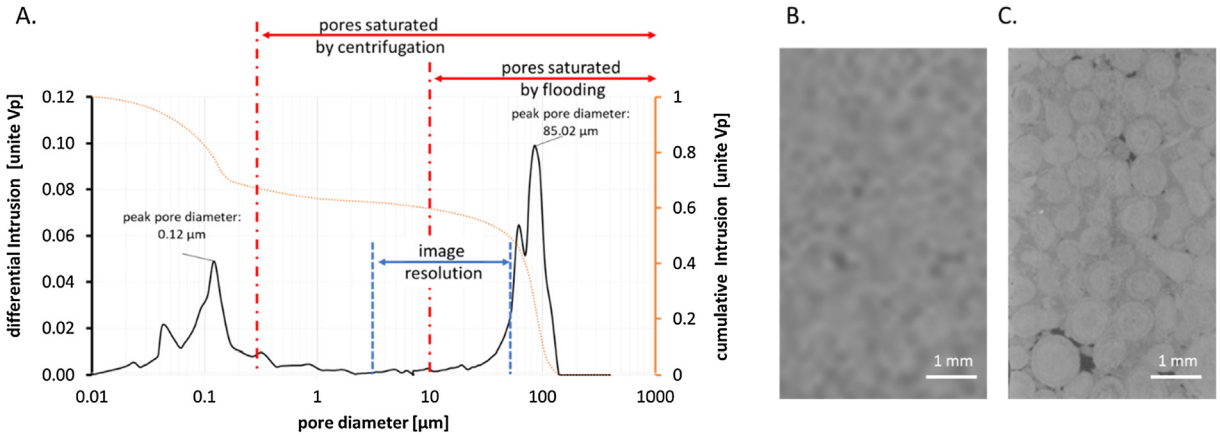

Fig. 4. (A) shows the pore size distribution of Ketton rock in unite pore volume (V_p) and includes an indication which pores are expected to be filled respectively by centrifugation and flooding (adapted from [88]). (B) shows a cross-sectional μCT image of the centrifuged sample (pixel length: 13 μm) and (C) the image of the sample initialized by flooding (pixel length: 6 μm). Both samples show a homogeneous distribution of the oil phase with only little trapped water.

appearance. Al-Raoush [106] confirmed a relationship between surface roughness and wetting within a different rock. However, the resolution of μCT is not sufficient to fully characterize the surface structure of the grains. In the following section, we, therefore, assess the impact of surface structure of the grains with AFM.

3.2. Surface roughness, disjoining pressure and capillary pressure

Fig. 5 shows the surface topography of a Ketton sample measured with AFM. The surface of Ketton is dominated by crystalline facets. The surface roughness, which was determined by the deviation of the measured surface from a quadratic fit mimicking the spherical shape of a Ketton grain, showed a symmetric distribution. Similar distributions were obtained at different locations in the same block in previous studies [98]. Based on this observation and due to the homogeneous nature of the rock, this surface is considered representative for the block. The average roughness of the surface was R_a = 1 μm, the root mean squared roughness of R_q = 1.3 μm and peak-to-valley roughness of R_t = 9.8 μm. This indicated that the roughness is higher than the size of fluid films, which for similar COBR systems was reported to be in the range from 1 to 150 nm [98,107]. Consequently, the roughness needs to be considered for the determination of the wetting state of the system [31]. However, these roughness indices tell little about the relationship of the surface structure to wetting.

More important than the actual roughness is the surface-oil contact at the drainage endpoint, as the rock surface -oil contact determines the location of wetting alteration [31]. As described above, the surface coverage will depend on the relationship between the global capillary pressure applied P_c^* and the disjoining pressure Π. Based on the augmented Young Laplace equation (IV), the water films break if the local capillary pressure P_c^{local}, which depends on the local curvature of the surface κ, exceeds the disjoining pressure Π^{max}. Fig. 6 shows the curvature of the rock surface (A) and the curvature distribution (B). The fluid films at the tips of the surface are highly convex ($\kappa < 0\ \mu m^{-1}$), while the valleys are highly concave ($\kappa > 0\ \mu m^{-1}$). Correspondingly, the fluid films would break first at the tips of the rock surface, while the valleys preserve the fluid films.

The disjoining pressure is COBR system dependent. For the disjoining pressure to be able to stabilize the film along a tip with a curvature of $\kappa = -5\ \mu m^{-1}$ for a range of global capillary pressure applied being $P_c^* < \sigma^{ob}\kappa^{min} + \Pi^{max}$, the maximum disjoining pressure Π^{max} must exceed 100 kPa. Other studies reported maximum disjoining pressures Π^{max} ranging from 30 kPa to negative values [50,51]. Fig. 6C (P_c^{local} = 0 kPa) displays the disjoining pressure - film thickness relationship, which was derived from ζ-measurements for the COBR system used in this study. The results show a negative disjoining pressure for all film thickness, which is in line with observations reported for various carbonates using similar crude oil and brine compositions [51]. The P_c^* - film thickness relationships plotted for P_c^{local} = 20 kPa, which corresponds to the valleys with a curvature of $\kappa = 1\ \mu m^{-1}$ along the rock surface, and P_c^{local} = −20 kPa, which correspond to asperities with a curvature of $\kappa = -1\ \mu m^{-1}$ illustrate how the fluid film would be affected by a variation in capillary pressure. The films are unstable at any location the surface shows a curvature $\kappa < 0\ \mu m^{-1}$. Only in asperities with a curvature $\kappa > 0\ \mu m^{-1}$, the fluid films remain maintained.

For the COBR system investigated, the water films remain stable if $P_c^* < \sigma^{ob}\kappa^{min}$, which means, that for estimations of surface area coverage, disjoining pressure can be neglected. Consequently, the surface area coverage by the wetting fluid can be estimated with the Young Laplace equation III and simulated with a sphere fitting algorithm based drainage simulation provided by GeoDICT [108]. The algorithm fits spheres of different radii, representing different capillary pressures, into the system. Thereby it considers the connectivity of the imbibing and the drained fluid, as trapped fluid cannot move. In this study we used the topographical image obtained with AFM as input defining the rock structure. For the studied system a water-wet contact angle of 30° was assumed. Fig. 7 illustrates the surface coverage of the rock (brown) by brine (blue) for different capillary pressures. At low capillary pressure little rock surface is exposed to oil, but as the capillary pressure increases, the coverage of the rock surface increases.

The rock surface exposed to oil appears patchy and disconnected, while the water forms connected streamlines through the valleys. As the capillary pressure P_c^* increases, the water gets drained through the water layers in the valleys of the surface structure (corner flow) down to 100% coverage with oil.

The resulting wetting pattern, which would be established after ageing would lead to pinning of the fluid-fluid interface as it moves along the surface and therefore impacts pore-scale flow regimes [105].

Fig. 8 puts the surface coverage, capillary pressure and the saturation in relation to each other. Combined with the topology of this system these values represent the 4 Minkowski functionals. At this length scale, however, the field of view is much smaller than a pore which away from the rock surface is occupied solely by oil, resulting in a Euler characteristic for the oil phase of 1. Fig. 8A displays the capillary pressure -saturation function obtained from MICP and Fig. 8B the capillary pressure -surface coverage function derived from the simulation. For the same capillary pressure range in which a change of 90% in surface coverage by oil was detected, only a minor change in saturation was obtained.

Yet, only the rock surface in direct contact with the oil is expected to alter its wetting state. So even though the saturation does not change significantly, the difference in capillary pressure indicates a significant shift from water-wet to oil-wet.

The dotted line represents the range of drainage capillary pressures at which the core scale samples were aged (Section 3.1,

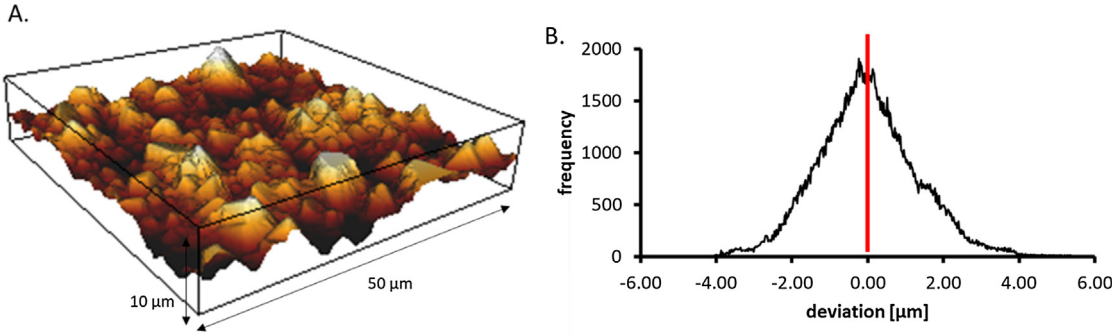

Fig. 5. The surface topology of Ketton rock is dominated by crystal facies of different orientations (A). The crystalline structure causes a height variation of up to 9.8 μm, with an average roughness of R_a = 1 μm.

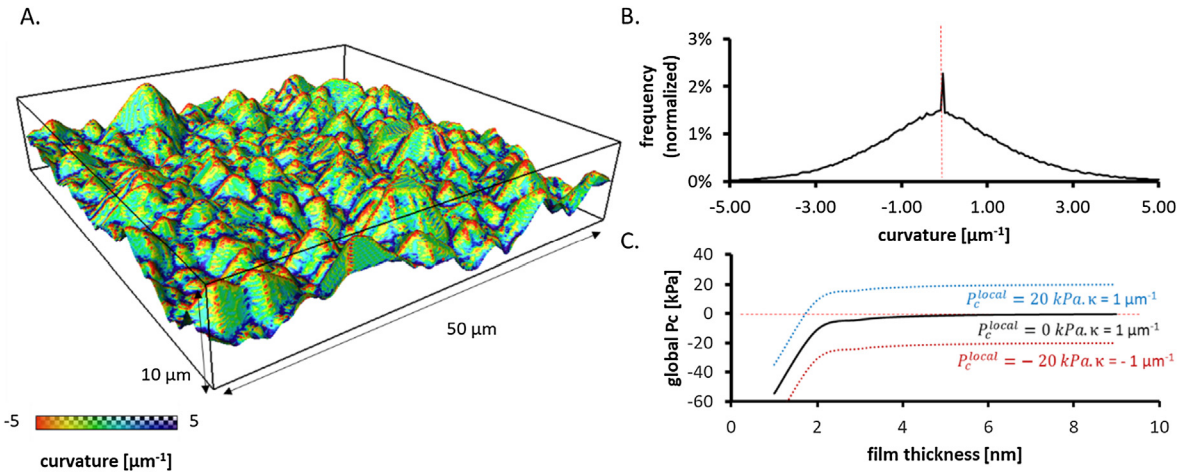

Fig. 6. A shows the curvature of the rock surface and B the associated curvature distribution. The crystal structures show a curvature of $-5\ \mu m^{-1}$ at their peaks, which corresponds to $-\sigma^{ob}\ \kappa = 100$ kPa. The COBR-system must show a maximum disjoining pressure Π^{max} smaller than this value to get a surface oil contact in the rock. The global capillary pressure film thickness relationships plotted for locations of different curvatures ($\kappa = 1\ \mu m^{-1}$, $\kappa = 0\ \mu m^{-1}$, $\kappa = -1\ \mu m^{-1}$) illustrates how the fluid film would be affected by curvature for the studied COBR system (C). The plot for $\kappa = 0\ \mu m^{-1}$, corresponds to the disjoining pressure – film thickness-relationship for the COBR-system as $P_c^{local} = 0$.

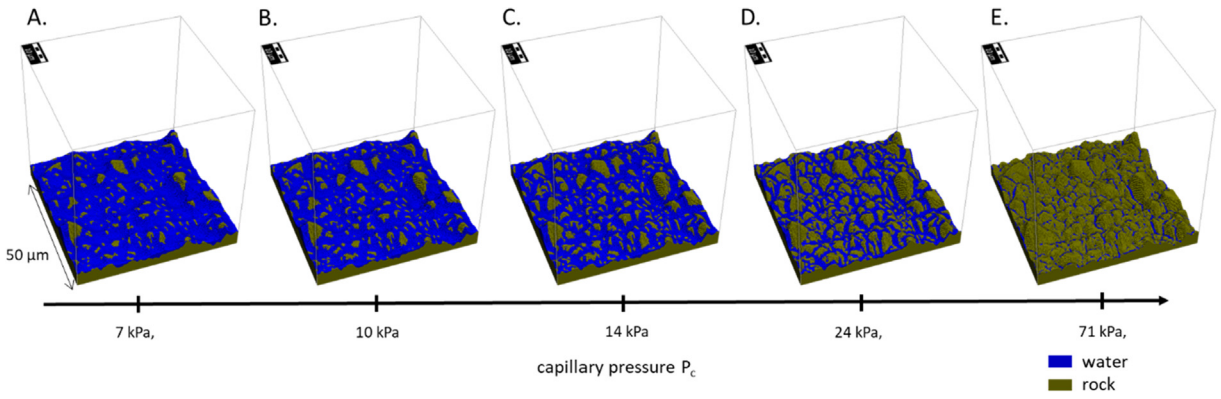

Fig. 7. Surface area coverage by brine (blue) and oil (transparent) along the rock surface (brown) for increasing capillary pressure (A: 7 kPa, B: 10 kPa, C: 14 kPa, D: 24 kPa, E: 71 kPa,) modelled with the sphere fitting algorithm from GeoDICT.

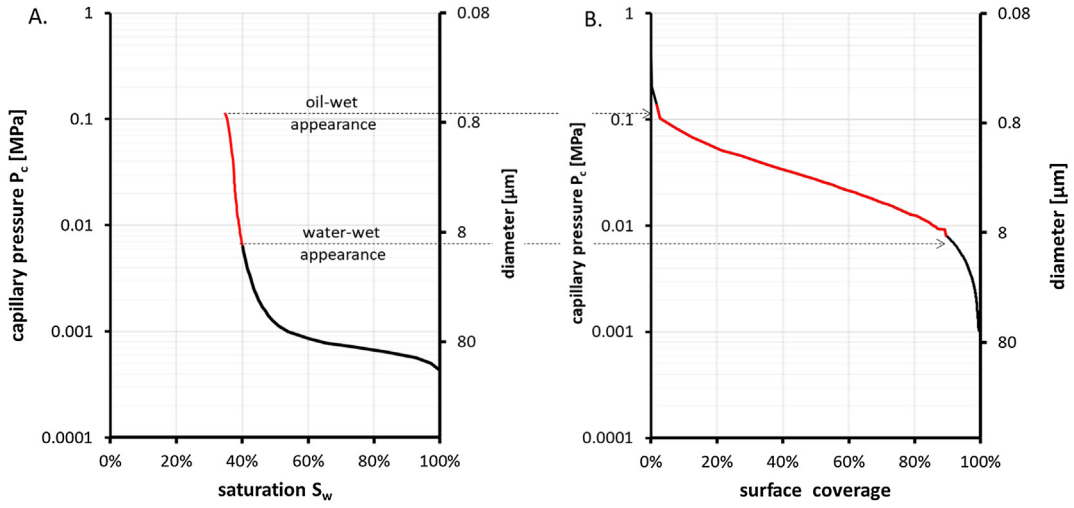

Fig. 8. A Capillary pressure vs. saturation function, B: Capillary pressure vs. surface coverage function.

Fig. 4). The capillary pressure- saturation relationship, indicates only small differences in saturation and common models considering solely pore sizes and shapes would predict a similar wetting response at the core scale [30]. However, the capillary pressure - surface area coverage relationship illustrates that in the same capillary pressure range, surface area coverage ranges from almost 100% oil to up to 90% water contact. As the oil-rock contact determines, where and how much of the rock surface gets altered, this relationship needs to be considered when linking molecular scale wetting properties with core-scale investigations.

From a conceptual perspective, this finding is key to link molecular wetting with the fluid-distributions observed during two-phase flow at larger scales. As the fluid distribution is considered to control the wetting alteration processes, all 4 Minkowski functionals after drainage need to be determined. The volume is given through the saturation, curvature through capillary pressure and the connectivity (Euler characteristic) is not expected to change when considering surface roughness. Correspondingly surface area or surface area coverage is the missing parameter.

This study demonstrates that the impact of the nano-scale surface roughness controls the wettability distributions along the rock surface. Furthermore, it connects the nano-scale wetting state to the perceived core-scale wetting. In order to predict the wetting response at the core-scale, the relationship between capillary pressure, saturation and surface area coverage needs to be investigated. Atomic force microscopy allows us to obtain the necessary resolution when μCT resolution is insufficient.

4. Conclusion

The results obtained at the core- and nano-scale show that the core-scale wetting response of the system strongly depends on surface area coverage by oil controlled by the surface structure of the grain surfaces and the capillary pressure applied during initialization. This relationship was conceptually discussed in many previous studies [26–31] and indicatively supported by pore- and Darcy-scale flow experiments [25,26]. However, though conceptually understood so far, a direct link to upscale molecular scale characteristics to flow behaviour in porous media attributing for surface properties such as roughness remained missing. With this paper, we introduced a novel systematic workflow to characterize the relevant surface attributes and demonstrated that the effect of roughness can be assessed through surface coverage - capillary pressure relationships.

In this study, we presented two core-scale experiments with the same crude oil, brine rock system, in which when high capillary pressure was applied, the rock sample appeared oil-wet but was water-wet for low capillary pressure initialization. The pore-occupancy by oil after drainage resolved by μCT was almost the same. The dependence of the wetting response on the surface structure of Ketton rock was assessed with atomic force microscopy, ζ-potential measurements and a static drainage simulation. The results demonstrate that surface coverage by oil varies from >80% even though the change in saturation is minor. Considering that the surface – oil contact is controlling the wetting alteration processes, we concluded that surface area coverage variation is responsible for the change in the core-scale wetting response.

Moving forward, the relationship between capillary pressure and surface area coverage needs to be considered next to the chemical interactions within the fluid/fluid/solid system for the development of predictive capability about wetting alteration. Complemented by mercury intrusion capillary pressure - saturation data and the Euler characteristic which can be derived from μCT images of the core, these descriptors would give the full set of Minkowski-functionals necessary to describe the 3D distribution of the oil-phase during wetting alteration.

Declaration of Competing Interest

The authors declare that they have no known competing financial interests or personal relationships that could have appeared to influence the work reported in this paper.

Acknowledgements

We would like to acknowledge UGCT, Ghent, Belgium for support for the spontaneous imbibition experiment. Furthermore, we would like to acknowledge Alex Schwing and Rob Neiteler for the design of the setup and instrumentation, Hilbert van der Linde for sample preparation. Jos Pureveen, Willie Schermer and Len van Gelder for characterizing the crude oil. Ryan Armstrong and James McClure, Matthew Leivers, Tannaz Pak, Frans Korndorffer, Ove Wilson, the Shell Digital Rock team at Imperial and Shell and the team from Math2Market for helpful discussions. We gratefully acknowledge Shell Global Solutions International B.V., Netherlands for funding and permission to publish this work.

The spontaneous imbibition data is available from Bartels et al. [109]: (https://www.digitalrocksportal.org/projects/188).

The surface structure of Ketton rock from Rücker et al. [113]: (https://www.digitalrocksportal.org/projects/231).

References

[1] I. Tanaka, M. Koishi, K. Shinohara, Evaluation of the wettability of spherical cement particle surfaces using penetration rate method, Cem. Concr. Res. 32 (7) (2002) 1161–1168.
[2] A.K. Singhal, D.P. Mukherjee, W.H. Somerton, Effect of heterogeneous wettability on flow of fluids through porous media, J. Can. Pet. Technol. 15 (03) (1976) 9.
[3] F.M. Orr, J.J. Taber, Use of carbon dioxide in enhanced oil recovery, Science 224 (4649) (1984) 563–569.
[4] Y.-W. Yang, G. Zografi, E.E. Miller, Capillary flow phenomena and wettability in porous media: II. Dynamic flow studies, J. Colloid Interface Sci. 122 (1) (1988) 35–46.
[5] G.H. de Rooij, Modeling fingered flow of water in soils owing to wetting front instability: a review, J. Hydrol. 231–232 (2000) 277–294.
[6] S. Gruener, Z. Sadjadi, H.E. Hermes, A.V. Kityk, K. Knorr, S.U. Egelhaaf, H. Rieger, P. Huber, Anomalous front broadening during spontaneous imbibition in a matrix with elongated pores, Proc. Natl. Acad. Sci. 109 (26) (2012) 10245–10250.
[7] M. Alava, M. Dubé, M. Rost, Imbibition in disordered media, Adv. Phys. 53 (2) (2004) 83–175.
[8] T. Pak, N.L. Archilha, R. Al-Imari, Application of nanotechnology in removal of NAPLs from contaminated aquifers: a source clean-up experimental study, Clean Technol. Environ. Policy 20 (2) (2018) 427–433.
[9] M.L. Brusseau, Rate-limited mass transfer and transport of organic solutes in porous media that contain immobile immiscible organic liquid, Water Resour. Res. 28 (1) (1992) 33–45.
[10] J. Murison, B. Semin, J.-C. Baret, S. Herminghaus, M. Schröter, M. Brinkmann, Wetting heterogeneities in porous media control flow dissipation, Phys. Rev. Appl. 2 (3) (2014) 034002.
[11] W. Abdallah, J.S. Buckley, A. Carnegie, J. Edwards, B. Herold, E. Fordham, A. Graue, T. Habashy, N. Seleznev, C. Signer, Fundamentals of wettability, Schlumberger Oilfield Rev. 19 (2) (2007) 44–61.
[12] E.C. Donaldson, W. Alam, in: *CHAPTER 1 - Wettability*, in *Wettability*, Gulf Publishing Company, 2008, pp. 1–55.
[13] R.J.S. Brown, I. Fatt, *Measurements Of Fractional Wettability Of Oil Fields' Rocks By The Nuclear Magnetic Relaxation Method*, in *Fall Meeting of the Petroleum Branch of AIME*, Los Angeles, California, 1956.
[14] R.A. Salathiel, Oil recovery by surface film drainage in mixed-wettability rocks, J. Petrol. Technol. 25 (10) (1973) 1216–1224.
[15] W. Anderson, Wettability literature survey – part 1: rock/oil/brine interactions and the effects of core handling on wettability, J. Petrol. Technol. 38 (10) (1986) 1125–1144.
[16] E. Amott, Observations Relating to the Wettability of Porous Rock, Petroleum Transactions, AIME, 1959, 216, pp. 156-132.
[17] S. Zou, R. Armstrong, Multiphase flow under heterogeneous wettability conditions studied by special core analysis and pore-scale imaging, SPE J. 24 (03) (2019) 1234–1247.
[18] K.S. Schmid, S. Geiger, Universal scaling of spontaneous imbibition for arbitrary petrophysical properties: water-wet and mixed-wet states and Handy's conjecture, J. Petrol. Sci. Eng. 101 (2013) 44–61.
[19] E.C. Donaldson, R.D. Thomas, P.B. Lorenz, Wettability determination and its effect on recovery efficiency, SPE J. 9 (01) (1969) 13–20.

[20] C. Zahasky, S.M. Benson, Spatial and temporal quantification of spontaneous imbibition, Geophys. Res. Lett. 46 (2019).
[21] N.S. Al Maskari, A. Sari, A. Saeedi, Q. Xie, Influence of surface roughness on the contact angle due to calcite dissolution in an oil–brine–calcite system: a nanoscale analysis using atomic force microscopy and geochemical modeling, Energy Fuels 33 (5) (2019) 4219–4224.
[22] S. Herminghaus, Wetting, spreading, and adsorption on randomly rough surfaces, Europ. Phys. J. E 35 (6) (2012) 43.
[23] S. Herminghaus, Universal phase diagram for wetting on mesoscale roughness, Phys. Rev. Lett. 109 (23) (2012) 236102.
[24] H. Mahani, S. Berg, D. Ilic, W.-B. Bartels, V. Joekar-Niasar, Kinetics of low-salinity-flooding effect, SPE J. 20 (01) (2015) 8–20.
[25] A. AlRatrout, M.J. Blunt, B. Bijeljic, Wettability in complex porous materials, the mixed-wet state, and its relationship to surface roughness, Proc. Natl. Acad. Sci. 115 (36) (2018) 8901–8906.
[26] S.K. Masalmeh, X. Jing, Improved characterisation and modelling of carbonate reservoirs for predicting waterflood performance, in: International Petroleum Technology Conference, Dubai, U.A.E., 2007, p. 14.
[27] M.D. Jackson, D. Al-Mahrouqi, J. Vinogradov, Zeta potential in oil-water-carbonate systems and its impact on oil recovery during controlled salinity water-flooding, Sci. Rep. 6 (2016) 37363.
[28] H.-J. Butt, Capillary forces: influence of roughness and heterogeneity, Langmuir 24 (9) (2008) 4715–4721.
[29] R. Lenormand, C. Zarcone, *Role of roughness and edges during imbibition in square capillaries*, in: *SPE Annual Technical Conference and Exhibitio*, Houston, Texas, 1984.
[30] P.H. Valvatne, M.J. Blunt, Predictive pore-scale modeling of two-phase flow in mixed wet media, Water Resour. Res. 40 (7) (2004) W07406.
[31] A.R. Kovscek, H. Wong, C.J. Radke, A pore-level scenario for the development of mixed wettability in oil reservoirs, AIChE J. 39 (6) (1993) 1072–1085.
[32] R. Bailey, V.R. Gray, Contact angle measurements of water on coal, J. Appl. Chem. 8 (4) (1958) 197–202.
[33] M.E. Schrader, S. Yariv, Wettability of clay minerals, J. Colloid Interface Sci. 136 (1) (1990) 85–94.
[34] F.C. Benner, W.W. Riches, F.E. Bartell, *Nature and importance of surface forces in production of petroleum*, in: *Drilling and Production Practice*, Amarillo, Texas, 1938.
[35] T. Hassenkam, L.L. Skovbjerg, S.L.S. Stipp, Probing the intrinsically oil-wet surfaces of pores in North Sea chalk at subpore resolution, Proc. Natl. Acad. Sci. 106 (15) (2009) 6071–6076.
[36] W. Anderson, Wettability literature survey – part 2: wettability measurement, J. Petrol. Technol. 38 (11) (1986) 1246–1262.
[37] M.A. Fernø, M. Torsvik, S. Haugland, A. Graue, Dynamic laboratory wettability alteration, Energy Fuels 24 (7) (2010) 3950–3958.
[38] C. Drummond, J. Israelachvili, Fundamental studies of crude oil–surface water interactions and its relationship to reservoir wettability, J. Petrol. Sci. Eng. 45 (1–2) (2004) 61–81.
[39] K. Kumar, E. Dao, K. Mohanty, Atomic force microscopy study of wettability alteration, in: SPE International Symposium on Oilfield Chemistry, The Woodlands, Texas, USA, 2005.
[40] J.S. Buckley, Effective wettability of minerals exposed to crude oil, Curr. Opin. Colloid Interface Sci. 6 (3) (2001) 191–196.
[41] G.V. Chilingar, T.F. Yen, Some notes on wettability and relative permeabilities of carbonate reservoir rocks, Energy Sources 7 (1) (1983) 67–75.
[42] L.E. Treiber, W.W. Owens, A laboratory evaluation of the wettability of fifty oil-producing reservoirs, SPE J. 12 (06) (1972) 531–540.
[43] T. Hassenkam, J. Mathiesen, C. Pedersen, K. Dalby, S. Stipp, I.R. Collins, Observation of the low salinity effect by atomic force adhesion mapping on reservoir sandstones, in: SPE Improved Oil Recovery Symposium, Oklahoma, USA, 2012.
[44] W.B. Bartels, H. Mahani, S. Berg, S.M. Hassanizadeh, Literature review of low salinity waterflooding from a length and time scale perspective, Fuel 236 (2019) 338–353.
[45] P. Purswani, M.S. Tawfik, Z.T. Karpyn, Factors and mechanisms governing wettability alteration by chemically tuned waterflooding: a review, Energy Fuels 31 (8) (2017) 7734–7745.
[46] J.T.G. Overbeek, E. Verwey, Theory of the Stability of Lyophobic Colloids: The interaction of Sol Particles Having an Electric Double Layer, Elsevier Publishing Company, New York-Amsterdam, 1948.
[47] B. Derjaguin, L. Landau, Theory of the stability of strongly charged lyophobic sols and of the adhesion of strongly charged particles in solutions of electrolytes, Acta Phys. Chim. URSS 14 (633) (1941).
[48] G.J. Hirasaki, Wettability: fundamentals and surface forces, SPE Form. Eval. 6 (02) (1991) 217–226.
[49] J.N. Israelachvili, Chapter 14 – Electrostatic Forces between Surfaces in Liquids, in: Intermolecular and Surface Forces, third ed., Academic Press, San Diego, 2011, pp. 291–340.
[50] S. Basu, M.M. Sharma, Measurement of critical disjoining pressure for dewetting of solid surfaces, J. Colloid Interface Sci. 181 (2) (1996) 443–455.
[51] H. Mahani, R. Menezes, S. Berg, A. Fadili, R. Nasralla, D. Voskov, V. Joekar-Niasar, Insights into the impact of temperature on the wettability alteration by low salinity in carbonate rocks, Energy Fuels 31 (8) (2017) 7839–7853.
[52] S. Ma, N. Morrow, X. Zhang, Generalized scaling of spontaneous imbibition data for strongly water-wet systems, J. Petrol. Sci. Eng. 18 (3–4) (1997) 165–178.
[53] C. Spurin, T. Bultreys, B. Bijeljic, M.J. Blunt, S. Krevor, Intermittent fluid connectivity during two-phase flow in a heterogeneous carbonate rock, Phys. Rev. E 100 (4) (2019) 043103.
[54] A.Z. Al-Yaseri, M. Lebedev, S.J. Vogt, M.L. Johns, A. Barifcani, S. Iglauer, Pore-scale analysis of formation damage in Bentheimer sandstone with in-situ NMR and micro-computed tomography experiments, J. Petrol. Sci. Eng. 129 (2015) 48–57.
[55] S.M. Shah, F. Gray, J.P. Crawshaw, E.S. Boek, Micro-computed tomography pore-scale study of flow in porous media: effect of voxel resolution, Adv. Water Resour. 95 (2016) 276–287.
[56] Q. Lin, B. Bijeljic, R. Pini, M.J. Blunt, S. Krevor, Imaging and measurement of pore-scale interfacial curvature to determine capillary pressure simultaneously with relative permeability, Water Resour. Res. 54 (9) (2018) 7046–7060.
[57] M. Andrew, B. Bijeljic, M.J. Blunt, Pore-scale contact angle measurements at reservoir conditions using X-ray microtomography, Adv. Water Resour. 68 (2014) 24–31.
[58] K. Singh, H. Menke, M. Andrew, Q. Lin, C. Rau, M.J. Blunt, B. Bijeljic, Dynamics of snap-off and pore-filling events during two-phase fluid flow in permeable media, Sci. Rep. 7 (2017) 5192.
[59] G. Myers, T. Varslot, A. Kingston, A. Herring, A. Sheppard, Ground-truth verification of dynamic x-ray micro-tomography images of fluid displacement, in: SPIE Optical Engineering + Applications. San Diego, USA, 2012.
[60] S. Iglauer, A. Paluszny, C.H. Pentland, M.J. Blunt, Residual CO2 imaged with X-ray micro-tomography, Geophys. Res. Lett. 38 (21) (2011) L21403.
[61] D. Wildenschild, A.P. Sheppard, X-ray imaging and analysis techniques for quantifying pore-scale structure and processes in subsurface porous medium systems, Adv. Water Resour. 51 (2013) 217–246.
[62] D. Wildenschild, K.A. Culligan, B.S.B. Christensen, Application of x-ray microtomography to environmental fluid flow problems, in: Optical Science and Technology, the SPIE 49th Annual Meeting, Denver, USA, 2004.
[63] A. Scanziani, K. Singh, T. Bultreys, B. Bijeljic, M.J. Blunt, In situ characterization of immiscible three-phase flow at the pore scale for a water-wet carbonate rock, Adv. Water Resour. 121 (2018) 446–455.
[64] K.J. Dobson, S.B. Coban, S.A. McDonald, J.N. Walsh, R.C. Atwood, P.J. Withers, 4-D imaging of sub-second dynamics in pore-scale processes using real-time synchrotron X-ray tomography, Solid Earth 7 (4) (2016) 1059–1073.
[65] T. Bultreys, M.A. Boone, M.N. Boone, T. De Schryver, B. Masschaele, D. Van Loo, L. Van Hoorebeke, V. Cnudde, Real-time visualization of Haines jumps in sandstone with laboratory-based microcomputed tomography, Water Resour. Res. 51 (10) (2015) 8668–8676.
[66] R.T. Armstrong, J.E. McClure, M.A. Berrill, M. Rücker, S. Schlüter, S. Berg, Beyond Darcy's law: the role of phase topology and ganglion dynamics for two-fluid flow, Phys. Rev. E 94 (4) (2016) 043113.
[67] S. Berg, H. Ott, S.A. Klapp, A. Schwing, R. Neiteler, N. Brussee, A. Makurat, L. Leu, F. Enzmann, J.-O. Schwarz, Real-time 3D imaging of Haines jumps in porous media flow, Proc. Natl. Acad. Sci. 110 (10) (2013) 3755–3759.
[68] A.C. Thompson, Minkowski Geometry, vol. 63, Cambridge University Press, Cambridge, 1996.
[69] H. Hadwiger, Vorlesungen über Inhalt, Oberfläche und Isoperimetrie, vol. 93, Springer-Verlag, Berlin, Goettingen, Heidelberg, Germany, 1957.
[70] S. Hyde, I. Barnes, B. Ninham, Curvature energy of surfactant interfaces confined to the plaquettes of a cubic lattice, Langmuir 6 (6) (1990) 1055–1062.
[71] K.R. Mecke, D. Stoyan, Statistical Physics and Spatial Statistics: The Art of Analyzing and Modeling Spatial Structures and Pattern Formation, vol. 554, Springer Science & Business Media, Berlin, 2000.
[72] Z. Liu, A. Herring, V. Robins, R. Armstrong, Prediction of permeability from Euler characteristic of 3D images, in: International Symposium of the Society of Core Analysts, Viena, Austria, 2017.
[73] C. Scholz, F. Wirner, J. Götz, U. Rüde, G.E. Schröder-Turk, K. Mecke, C. Bechinger, Permeability of porous materials determined from the Euler characteristic, Phys. Rev. Lett. 109 (26) (2012) 264504.
[74] J.E. McClure, R.T. Armstrong, M.A. Berrill, S. Schlüter, S. Berg, W.G. Gray, C.T. Miller, Geometric state function for two-fluid flow in porous media, Phys. Rev. Fluids 3 (8) (2018) 084306.
[75] M. Rücker, S. Berg, R. Armstrong, A. Georgiadis, H. Ott, A. Schwing, R. Neiteler, N. Brussee, A. Makurat, L. Leu, From connected pathway flow to ganglion dynamics, Geophys. Res. Lett. 42 (10) (2015) 3888–3894.
[76] Z. Liu, A. Herring, C. Arns, S. Berg, R.T. Armstrong, Pore-scale characterization of two-phase flow using integral geometry, Transp. Porous Media 118 (1) (2017) 99–117.
[77] R.T. Armstrong, J.E. McClure, V. Robins, Z. Liu, C.H. Arns, S. Schlüter, S. Berg, Porous media characterization using minkowski functionals: theories, applications and future directions, Transp. Porous Media (2018).
[78] A.L. Herring, V. Robins, A.P. Sheppard, Topological persistence for relating microstructure and capillary fluid trapping in sandstones, Water Resour. Res. 55 (1) (2019) 555–573.
[79] S. Schlüter, S. Berg, M. Rücker, R.T. Armstrong, H.J. Vogel, R. Hilfer, D. Wildenschild, Pore-scale displacement mechanisms as a source of hysteresis for two-phase flow in porous media, Water Resour. Res. 52 (3) (2016) 2194–2205.
[80] A.L. Herring, A. Sheppard, L. Andersson, D. Wildenschild, Impact of wettability alteration on 3D nonwetting phase trapping and transport, Int. J. Greenhouse Gas Control 46 (2016) 175–186.

[81] A.L. Herring, E.J. Harper, L. Andersson, A. Sheppard, B.K. Bay, D. Wildenschild, Effect of fluid topology on residual nonwetting phase trapping: Implications for geologic CO2 sequestration, Adv. Water Resour. 62 (2013) 47–58.
[82] J.E. McClure, M.A. Berrill, W.G. Gray, C.T. Miller, Influence of phase connectivity on the relationship among capillary pressure, fluid saturation, and interfacial area in two-fluid-phase porous medium systems, Phys. Rev. E 94 (3) (2016) 033102.
[83] R.T. Armstrong, M.L. Porter, D. Wildenschild, Linking pore-scale interfacial curvature to column-scale capillary pressure, Adv. Water Resour. 46 (2012) 55–62.
[84] T. Li, S. Schlüter, M.I. Dragila, D. Wildenschild, An improved method for estimating capillary pressure from 3D microtomography images and its application to the study of disconnected nonwetting phase, Adv. Water Resour. 114 (2018) 249–260.
[85] A.L. Herring, J. Middleton, R. Walsh, A. Kingston, A. Sheppard, Flow rate impacts on capillary pressure and interface curvature of connected and disconnected fluid phases during multiphase flow in sandstone, Adv. Water Resour. 107 (2017) 460–469.
[86] Q. Lin, B. Bijeljic, S. Berg, R. Pini, M.J. Blunt, S. Krevor, Minimal surfaces in porous media: Pore-scale imaging of multiphase flow in an altered-wettability Bentheimer sandstone, Phys. Rev. E 99 (6) (2019) 063105.
[87] A. Scanziani, K. Singh, M.J. Blunt, A. Guadagnini, Automatic method for estimation of in situ effective contact angle from X-ray micro tomography images of two-phase flow in porous media, J. Colloid Interface Sci. 496 (2017) 51–59.
[88] W.-B. Bartels, M. Rücker, M. Boone, T. Bultreys, H. Mahani, S. Berg, S.M. Hassanizadeh, V. Cnudde, Imaging spontaneous imbibition in full Darcy-scale samples at pore-scale resolution by fast X-ray tomography, Water Resour. Res. 55 (2019) 7072–7085.
[89] A.M. Alhammadi, A. AlRatrout, K. Singh, B. Bijeljic, M.J. Blunt, In situ characterization of mixed-wettability in a reservoir rock at subsurface conditions, Sci. Rep. 7 (1) (2017) 10753.
[90] D. Quéré, Wetting and roughness, Annu. Rev. Mater. Res. 38 (1) (2008) 71–99.
[91] N.R. Morrow, The effects of surface roughness on contact: angle with special reference to petroleum recovery, J. Can. Pet. Technol. 14 (04) (1975) 0021–9487.
[92] N.R. Morrow, Capillary pressure correlations for uniformly wetted porous media, J. Can. Pet. Technol. 15 (04) (1976) 0021–9487.
[93] Y. Deng, L. Xu, H. Lu, H. Wang, Y. Shi, Direct measurement of the contact angle of water droplet on quartz in a reservoir rock with atomic force microscopy, Chem. Eng. Sci. 177 (2018) 445–454.
[94] Q. Lin, B. Bijeljic, S.C. Krevor, M.J. Blunt, M. Rücker, S. Berg, A. Coorn, H. van der Linde, A. Georgiadis, O.B. Wilson, A new waterflood initialization protocol with wettability alteration for pore-scale multiphase flow experiments, Petrophysics 60 (02) (2019) 264–272.
[95] E. Flügel, Microfacies of carbonate rocks: analysis, interpretation and application, Springer Science & Business Media, Berlin - Heidelberg, Germany, New York, US, 2013.
[96] M. Andrew, Reservoir-Condition Pore-Scale Imaging of Multiphase Flow, PhD Thesis, Imperial College, London, 2015.
[97] H. Mahani, A.L. Keya, S. Berg, W.-B. Bartels, R. Nasralla, W.R. Rossen, Insights into the mechanism of wettability alteration by low-salinity flooding (LSF) in carbonates, Energy Fuels 29 (3) (2015) 1352–1367.
[98] M. Rücker, Wettability and wettability alteration at the pore- and nano-scales, PhD Thesis, Imperial College London, 2018.
[99] R.J. Hunter, Zeta Potential in Colloid Science: Principles and Applications, vol. 2, Academic Press Limited, London, 2013.
[100] P. Zhang, T. Austad, Wettability and oil recovery from carbonates: effects of temperature and potential determining ions, Colloids Surf., A 279 (1) (2006) 179–187.
[101] G. Mason, N.R. Morrow, Developments in spontaneous imbibition and possibilities for future work, J. Petrol. Sci. Eng. 110 (2013) 268–293.
[102] S.M. Ma, X. Zhang, N.R. Morrow, X. Zhou, Characterization of Wettability from spontaneous imbibition measurements, in: Annual Technical Meeting Calgary, Alberta, Canada, 1999.
[103] T. Bultreys, W. De Boever, V. Cnudde, Imaging and image-based fluid transport modeling at the pore scale in geological materials: a practical introduction to the current state-of-the-art, Earth Sci. Rev. 155 (2016) 93–128.
[104] N. Alyafei, M.J. Blunt, The effect of wettability on capillary trapping in carbonates, Adv. Water Resour. 90 (2016) 36–50.
[105] M. Rücker, W.-B. Bartels, K. Singh, N. Brussee, A. Coorn, H.A. van der Linde, A. Bonnin, H. Ott, S.M. Hassanizadeh, M.J. Blunt, H. Mahani, A. Georgiadis, S. Berg, The effect of mixed wettability on pore-scale flow regimes based on a flooding experiment in ketton limestone, Geophys. Res. Lett. 46 (6) (2019) 3225–3234.
[106] R.I. Al-Raoush, Impact of wettability on pore-scale characteristics of residual nonaqueous phase liquids, Environ. Sci. Technol. 43 (13) (2009) 4796–4801.
[107] J. Schmatz, J.L. Urai, S. Berg, H. Ott, Nanoscale imaging of pore-scale fluid-fluid-solid contacts in sandstone, Geophys. Res. Lett. 42 (7) (2015) 2189–2195.
[108] M. Hilpert, C.T. Miller, Pore-morphology-based simulation of drainage in totally wetting porous media, Adv. Water Resour. 24 (3) (2001) 243–255.
[109] W.B. Bartels, M. Rücker, M. Boone, T. Bultreys, V. Cnudde, Spontaneous Imbibition, Digital Rocks Portal (2019).
[110] F. Mugele, I. Sirentanu, N. Kumar, B. Bera, L. Wang, R. de Ruiter, A. Maestro, M. Duits, D. van den Ende, I. Collins, Insights From Ion Adsorption and Contact-Angle Alteration at Mineral Surfaces for Low-Salinity Waterflooding, SPE Journal 21 (4) (2016) 1204–1213.
[111] B. Liang, I. Zarikos M., W.-B. Bartels, S. Hassanizadeh M., A. Clarens F., Effect of Nanoscale Surface Textures on Multiphase Flow Dynamics in Capillaries, Langmuir 35 (22) (2019) 7322–7331.
[112] C. Mattax C., J. Kyte R., Imbibition oil recovery from fractured, water-drive reservoir, SPE Journal 2 (2) (1962) 177–184.
[113] M. Rücker, P. Luckham F., Surface structure of Ketton rock, Digital Rocks Portal (2019).